Applied Surface Science 315 (2014) 252–260

Contents lists available at ScienceDirect

Applied Surface Science

journal homepage: www.elsevier.com/locate/apsusc

Selenium adsorption at different coverages on Fe(1 0 0) and Fe(1 1 1): A DFT study

V. Cardoso Schwindt[a], J.S. Ardenghi[a], P. Bechthold[a], E.A. González[a], P.V. Jasen[a], A. Juan[a,*], B.S. Batic[b], M. Jenko[b]

[a] Departamento de Física, Universidad Nacional del Sur & IFISUR (UNS-CONICET), Av. Alem 1253, (8000) Bahía Blanca, Argentina
[b] Institute of Metals and Technology, Lepipot 11, p.p. 431, SI-1001 Ljubljana, Slovenia

ARTICLE INFO

Article history:
Received 6 June 2014
Received in revised form 22 July 2014
Accepted 23 July 2014
Available online 30 July 2014

Keywords:
Iron surfaces
Electronic structure
Magnetic properties
Surface reconstruction
Selenium

ABSTRACT

Se adsorption on Fe(1 0 0) and (1 1 1) surfaces is examined using the density functional theory (DFT). Selenium is adsorbed in a distorted bridge on the (1 1 1) surface while in the (1 0 0) surface it prefers a 4-fold hollow site, with energies of −10.36 and −5.25 eV, respectively. Se adsorption results in surface reconstruction. There is some contraction in the case of the (1 0 0) plane for 1/4 and 1/2 ML coverage and some relaxation at 1 ML (4.5%). Contraction increases to 15% for the (1 1 1) plane at ¼ ML. At a higher coverage, there is a non-regular movement of surface metal atoms, and there is almost no change at 1 ML. The magnetic moment for surface Fe atoms decreases with coverage. The most important changes are in the (1 0 0) plane, followed by the (1 1 0) and then the (1 1 1) planes with a reduction of 52%, 24% and 7% respectively.

The density of states presents a contribution of Se states at −5.0 and −13.1 eV, when stabilized after adsorption. The Fe–Fe bond weakening is higher in the (1 0 0) plane. Fe–Se bonds are formed at the expense of the metallic bond.

1. Introduction

With the fast development of wireless communication applications and the widespread use of microwave devices over the 1–4 GHz range, the emerging hazards of microwaves and electrical equipment on human health have earned the interest of many researchers. Electromagnetic interference (EMI) shielding offers an effective way to solve the problem. Therefore, the manufacturing of absorbing/shielding materials will efficiently overcome the above mentioned problems. Incident microwaves are attenuated thanks to these materials and the microwaves reflected become much weaker as compared to the incident waves reflected from traditional shielding materials. At present, the absorbent is the key factor dominating absorbing and shielding properties [1]. FeSiAl alloys, soft metallic magnetic materials, have been extensively used as absorbing materials due to high saturation magnetization values and Snoek's limit at gigahertz (GHz) frequency ranges.

Fe–Si–Al alloys are also known as silicon steels. This type of steel is tailored to produce certain magnetic properties, such as a small hysteresis loop area and high permeability, as it is used for transformer cores and for electrical motor stator and rotor components. The microstructure of the steel consists of α-Fe grains (ferritic bcc structure) with some inclusions, depending on the composition [2]. Impurity elements in the steel, though added in very small concentrations, have a great effect on the final properties of the steel, and many of these are not thoroughly understood yet [3]. Fe planes in FeSiAl (D03 structure) have some similarities with bcc Fe surfaces. Fe_3A1_{1-x} Si_x alloys present (1 0 0) single planes formed only by Fe atoms where the Fe–Fe distance decrease from 2.48 to 2.42 Å when Si content increases [4]. The closer Fe–Fe distance in bcc structure is 2.47 Å [5].

It has been shown that a small addition of Se improves the texture and magnetic shielding properties of the FeSi alloys [6]. Se is a surface-active element that segregates to free surfaces at elevated temperatures (above 850 °C). X-ray photoelectron spectroscopy (XPS) studies show a correlation between Si and Se segregation in the form of co-segregation. No chemical bonding between the two elements has been observed in previous XPS studies [7]. Se also has a crucial effect on surface reconstruction and recrystallization as well as on the grain growth of individual crystal grains in the alloy. Upon surface segregation, roof-top-like morphologies form in the grains with observable amounts of Se segregated species.

Experimental data on Se adsorption is rather scarce while some data on sulphur are available. S surface structures – chemically

* Corresponding author. Tel.: +54 291 4595101x2818; fax: +54 0291 4595142.
E-mail address: cajuan@uns.edu.ar (A. Juan).

http://dx.doi.org/10.1016/j.apsusc.2014.07.131
0169-4332/

similar to Se – were experimentally determined on Fe by low electron energy diffraction (LEED) [8]. Spencer et al. examined the adsorption of atomic S on Fe(1 1 0) using density functional theory (DFT). They found that the hollow site with a relatively minor surface reconstruction was the most stable location for S [9]. The adsorption of atomic sulfur at different coverages on the Fe(1 1 0) surface was also examined using DFT in order to analyze the effect of adsorbate–adsorbate interactions [10,11]. The authors found that the bonding goes from being S–Fe dominated at low coverages to being S–S dominated at higher coverages where S atoms are located closer together on the surface and interact with each other [8]. Nelson et al. studied the effect of Fe(1 0 0) using DFT calculations [12]. S is found to adsorb mainly at hollow sites on the isolated surface in agreement with experiment.

Recently, DFT theoretical studies of elements belonging to the same group of Se and other atoms adsorbed on Fe surfaces was published [13–16]. Also, Çakmak et al. investigated the adsorption of Se on Si (0 0 1) [17].

Nakanishi and Horiguchi performed an experimental study of Se adsorption on bcc Fe(1 0 0) by LEED, Auger electron spectroscopy (AES), and work function changes (WFC). At 520 K they reported a p(1 × 1) structure of up to 0.1 ML, that changed to c(2 × 2) at a higher coverage [18].

To the best of our knowledge, there are only a few theoretical studies of Se adsorption on Fe surfaces. Anderson studied the

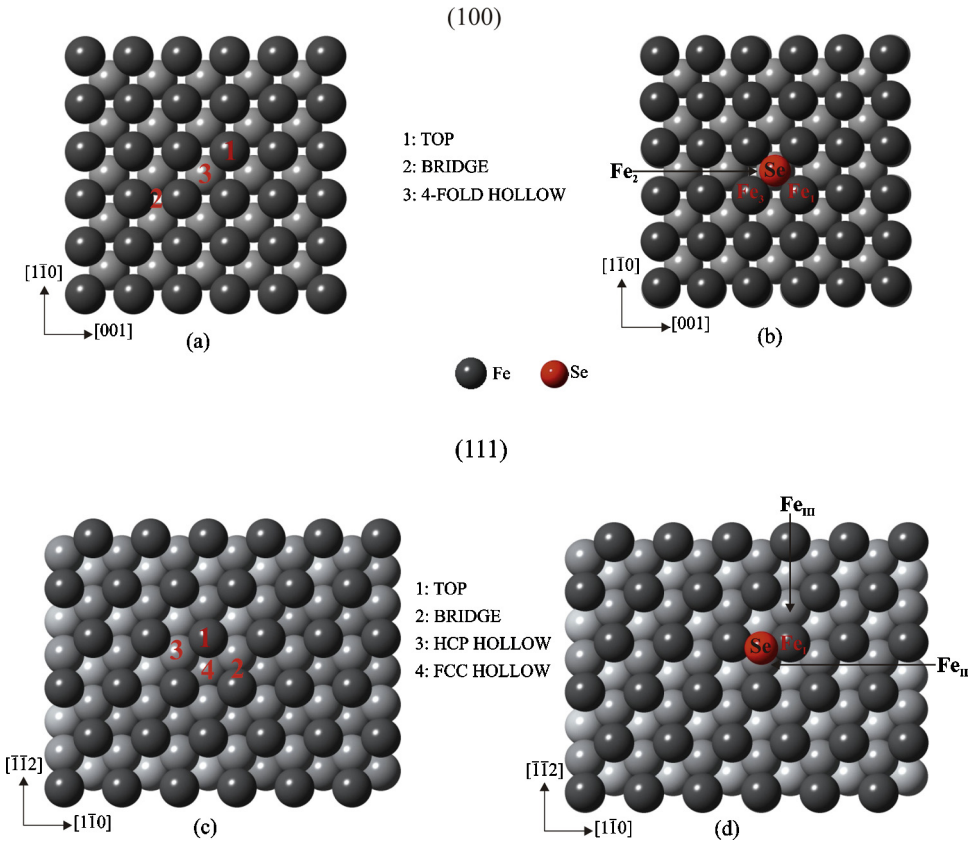

Fig. 1. Schematic top view of adsorption sites for the Fe(1 0 0) surface (a) and for the (1 1 1) plane (c). Top view of the most stable adsorption site for (1 0 0) (b) and (1 1 1) (d) surfaces.

Table 1
Atomic plane relaxation [$\Delta_{ij} = (d_{ij} - d)/d$], where d_{ij} is the distance between the ith and jth surface plane and $d = d^{hkl}$ is the interplanar spacing in bulk (in % of bulk spacing). Surface energy per unit area γ (J/m^2). Magnetic moment (in μ_B) per Fe atom in the top atomic layer and surface roughness ($S_r = A_{2D}/A_{Fe}$, where A_{2D} is the area of the surface unit cell and $A_{Fe} = (3/16\pi)a^2$ is the cross-sectional area of a hard ball representing a Fe atom in the bcc structure.).

Surface	(1 0 0)				(1 1 1)			
	Clean	1/4 ML	1/2 ML	1 ML	Clean	1/4 ML	1/2 ML	1 ML
γ	2.45 2.47[1]	–	–	–	2.61 2.58[1]	–	–	-
Δ_{12}	−5.4 −3.6[1] −5 ± 2[2]	(−1.7, −2.0)	−2.9	4.5	−26.9 −17.7[1] −29 ± 7[3]	(−6.7, −14.9)	−11.5, 14.7	1.0
μ_B	2.95 2.95[1]	2.77	2.36	1.42	2.75 2.81[1] 2.73[4]	2.71	2.68	2.56
S_r	1.72 1.70[1]	–	–	–	2.95 2.94[1]	–	–	–

[1] Ref. [41].
[2] Ref. [39].
[3] Ref. [40].
[4] Ref. [44].

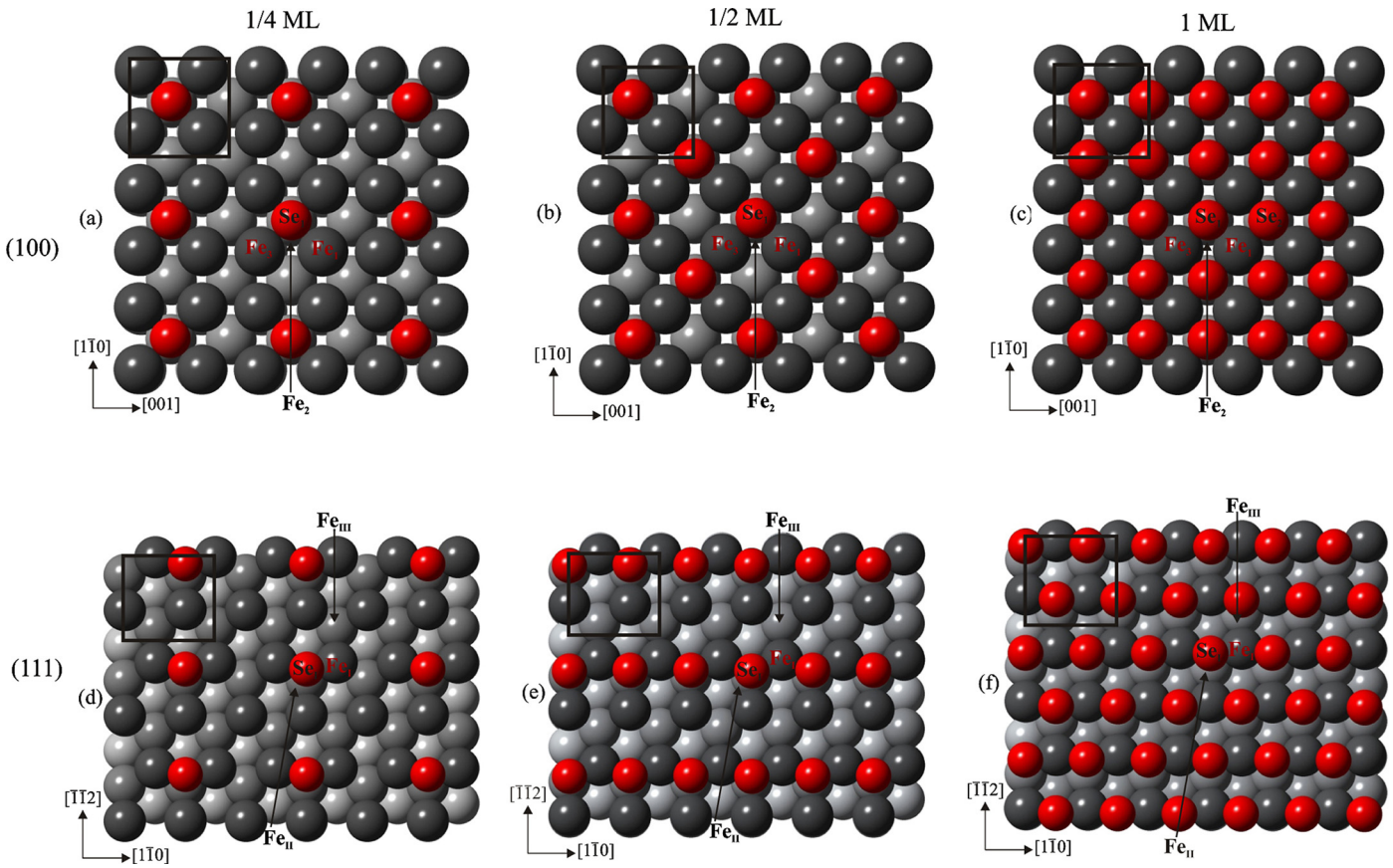

Fig. 2. Schematic top view of Se coverage on the Fe(1 0 0) surface: 1/4 ML (a); 1/2 ML (b), and 1 ML (c). Schematic top view of Se coverage on the Fe(1 1 1) surface: 1/4 ML (d); 1/2 ML (e), and 1 ML (f).

adsorption of Se, S, and acetylene on Fe and Ni (1 0 0) surfaces [19]. Gonzalez et al. by performing DFT calculations found Se located on a long-bridge site on Fe(1 1 0) at low coverage [20]. They also reported that the Se caused an ordered reconstruction and relaxation of the Fe surface.

The aim of the present work is to analyze the adsorption of Se in two low index bcc Fe surfaces: (1 0 0) and (1 1 1) and to compare with previous calculations on (1 1 0). We also computed changes in surface geometry, magnetic moment, electronic structure, and bonding after Se adsorption.

2. Theory and models

2.1. Computational details

Calculations were performed using the density functional theory (DFT) as implemented in the VASP code [21–23]. Exchange and correlation energies were calculated with the Perdew–Burke–Ernzerhof form of the spin-polarized generalized gradient approximation (GGA-PBE) [24]. Spin polarization and nonlinear core corrections were included in Fe system calculations so as to correctly account for its magnetic properties [25]. Spin polarization has been shown to have a major effect on the adsorption energies of magnetic systems and may alter the topology of potential energy surfaces [26]. The electron–ionic core interaction was represented by ultrasoft pseudopotentials [27]. A plane-wave basis with an energy cutoff of 330 eV was used to expand electronic wave functions. Brillouin zone integrations were performed on a special *k*-point mesh generated by the Monkhorst–Pack scheme ($12 \times 12 \times 12$ in bulk) [28]. In order to accelerate convergence, the first order Methfessel–Paxton method with a Fermi surface smearing of 0.2 eV was adopted for fractional occupancies [29]. The calculations for the bulk crystal structure give a lattice constant of bcc Fe equal to 2.846 Å (2.867 Å [30]), and the bulk modulus

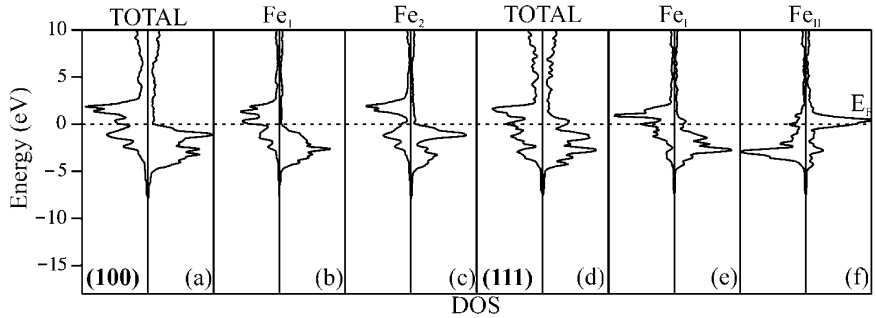

Fig. 3. Total DOS curves (a); projected DOS for a Fe_1 atom (b), for a Fe_2 atom (c), and for the Fe(1 0 0) surface. Total DOS curves (d); projected DOS for a Fe_I atom (b), for a Fe_{II} atom (c), and for the Fe(1 1 1) surface.

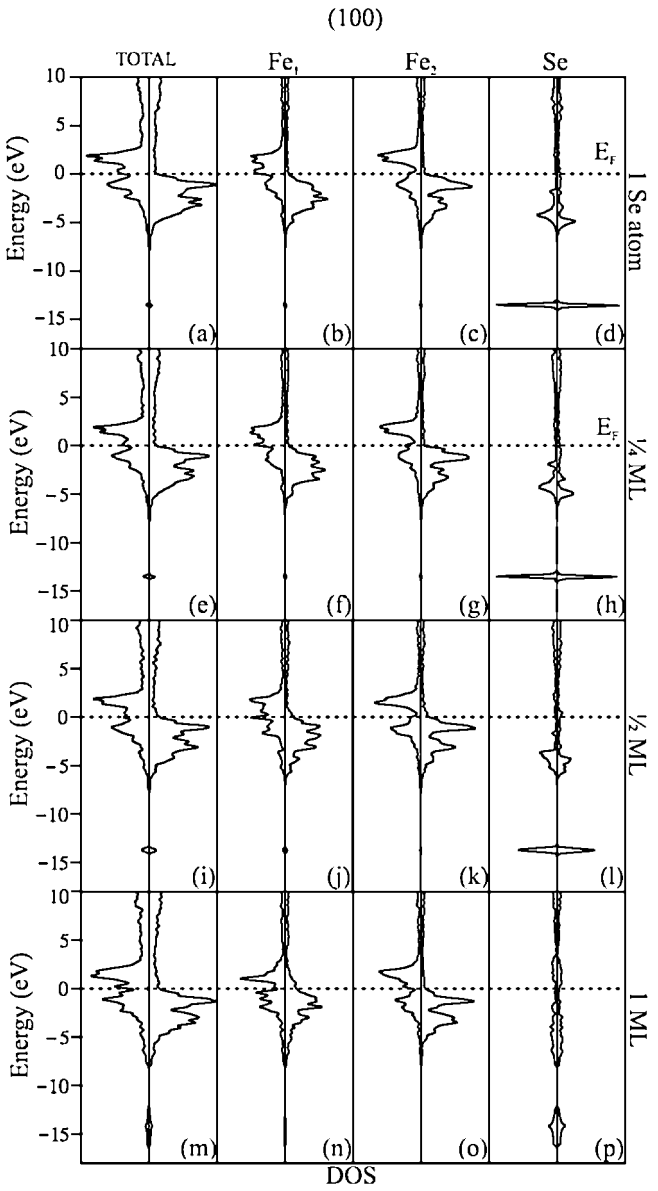

Fig. 4. Total DOS curves (a), (e), (i), and (m); projected DOS for a Fe_1 atom (b), (f), (j), and (n); projected DOS for a Fe_2 atom (c), (g), (k), and (o); and projected DOS for a Se atom (d), (h), (l), and (p) for the Fe(1 0 0) surface after Se adsorption.

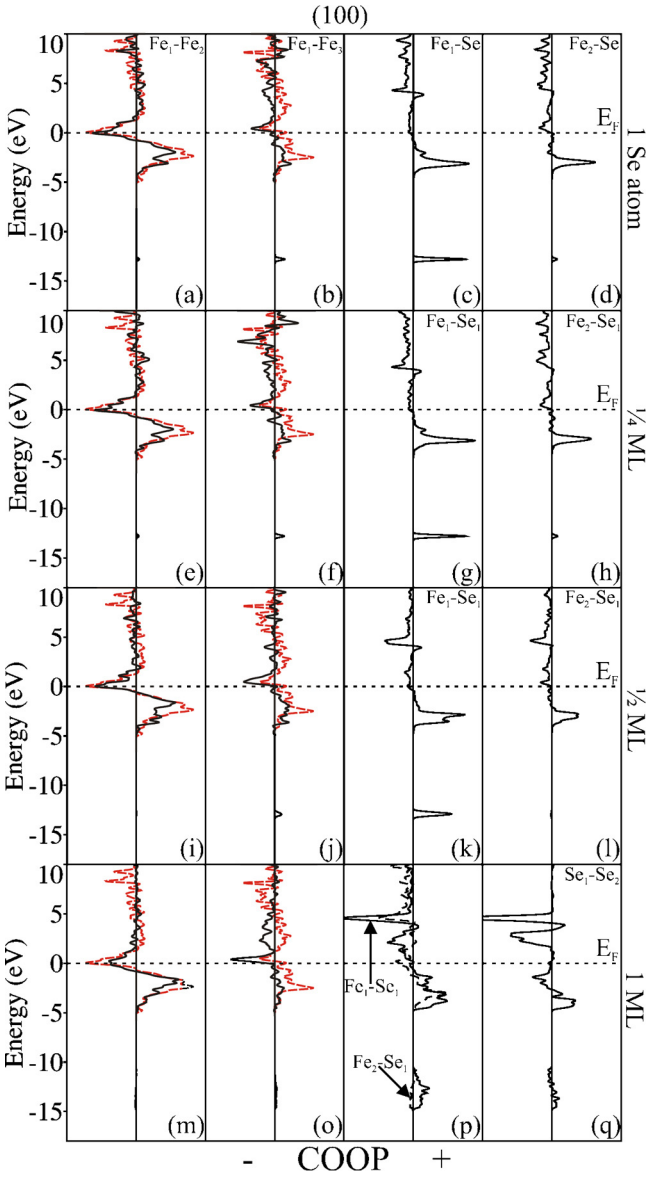

Fig. 5. COOP curves for the Fe_1–Fe_2 bond before (black solid line) and after Se adsorption (dotted red line) (a), Fe_1–Fe_3 bond before (black solid line) and after Se adsorption (dotted red line) (b), Fe_1–Se bond (c), and Fe_2–Se bond (d). (e)–(h) and (i)–(l) the same bonds at 1/4 and 1/2 ML, respectively. COOP curves for the Fe_1–Fe_2 bond before (black solid line) and after Se adsorption (dotted red line) (m), Fe_1–Fe_3 bond before (black solid line) and after Se adsorption (dotted red line) (n), Fe_1–Se and Fe_2–Se (p) and Se–Se (q) at 1 ML on Fe(1 0 0) (For interpretation of the color information in this figure legend, the reader is referred to the web version of the article.).

of 167 GPa (170 GPa [30]) is in full agreement with measured values (quoted between brackets). The local spin magnetic moment of $2.20\mu_B$ (Bohr magnetron) is in full agreement with previous calculations [31,32]. The approach used here is similar to that reported by Hung et al., giving a good description of bulk and ideal surface properties of bcc Fe [33]. Bader analysis was used to calculate magnetic moments and electronic charges on atoms [34].

2.2. Surface models

The surfaces considered were modeled by slabs consisting of several (up to 15) atomic layers of Fe separated by a vacuum layer of 15 Å, and periodically repeated throughout space. We used a k-point mesh of $8 \times 8 \times 1$ for both surfaces, which provided well-converged total energies. The positions of all atoms were fully optimized until the forces on each atom were less than 0.02 eV/Å. Test calculations for denser k-point meshes showed that the uncertainty of surface energies is within 0.01 J/m^2 and that of relaxations is within 0.5%.

For slab calculations, surface free energy σ was determined by

$$\sigma = \frac{1}{2}(E_m - E_B) \quad (1)$$

where E_m is the total energy of the m-layer slab, and E_B is the total energy of a single bulk layer. The 1/2 factor accounts for the presence of two surfaces. Experimentally relevant is the surface energy per unit area, γ, which is obtained by dividing σ by the area, A, of the surface unit cell. A direct application in Eq. (1) of the E_B determined from the self-consistent bulk calculations ($E_B = -8.20$ eV) leads to a linear divergence with the slab thickness [35,36]. In order to eliminate this problem for varying slab thicknesses, the bulk energy was calculated as the total energy increment of the relaxed slabs, $\Delta E_m = E^m_{\text{slab}} - E^{m-1}_{\text{slab}}$ [35]. An arithmetic average of the energy

increment ΔE_m, for slabs of 10–15 layers, calculated separately for each slab orientation, was taken as E_B.

In this work, selenium is adsorbed in the high-symmetry surface sites for each plane: bridge, atop, and 4-fold hollow sites for the (1 0 0) surface; bridge, atop, HCP, and FCC hollow sites for the (1 1 1) surface (see Fig. 1). We also studied different Se coverages (1/4, 1/2, and 1 ML), only in the most stable sites, in both surfaces (see Fig. 2). The adsorption energies were calculated using the following equation:

$$\Delta E_{ads} = \frac{[E_{slab+nSe} - E_{slab} - nE_{Se}]}{n} \quad (2)$$

Here, the first term on the right-hand side is the total energy for the Fe surface super cell plus n Se atoms, depending on the coverage. The second term is the total energy for the Fe super-cell; the third term is the Se atom total energy. This last term is calculated by placing a Se atom in a cubic box with 10 Å sides and carrying out a Γ-point calculation.

In order to understand Fe–Se interactions, we used the concepts of density of states (DOS) and crystal orbital overlap population (COOP). The DOS curve is a plot of the number of orbitals as a function of energy. The integral of the DOS curve over an energy interval gives the number of one-electron states in that interval; the integral up to the Fermi level (E_F) gives the total number of occupied molecular orbitals. If the DOS is weighed with the overlap population between two atoms, the COOP is obtained. The integration of the COOP curve up to E_F gives the total overlap population of the specified bond orbital and it is a measure of the bond strength. If an orbital at certain energy is strongly bonding between two atoms, the overlap population is strongly positive and the COOP curve will be large and positive around that energy. Similarly, negative COOP around certain energy corresponds to antibonding interactions. The COOP curves were computed using the SIESTA code [37,38].

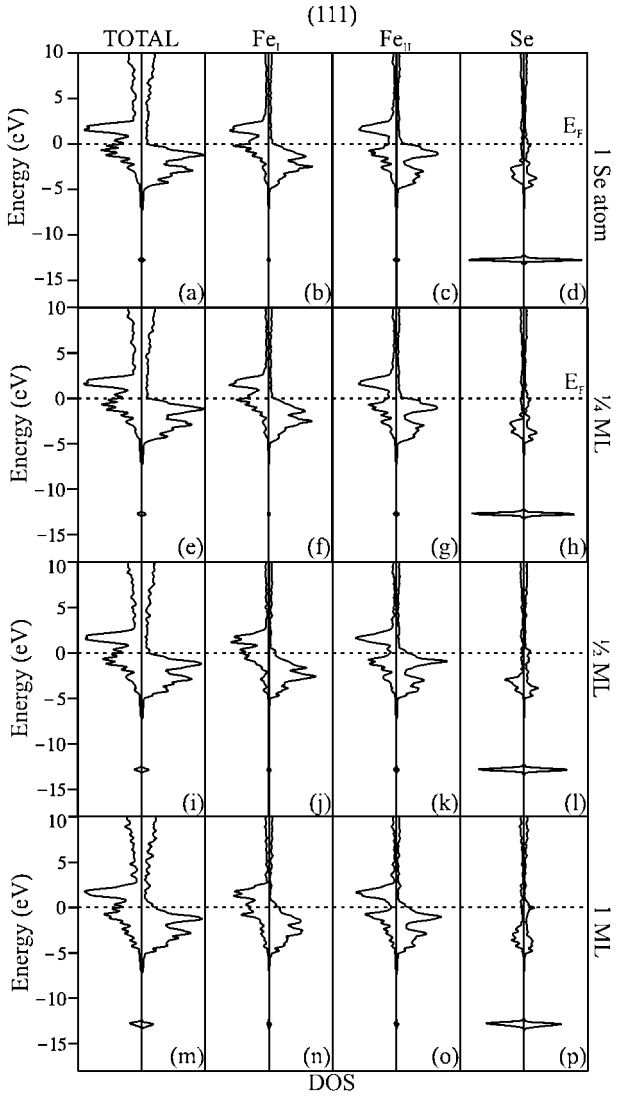

Fig. 6. Total DOS curves (a), (e), (i), and (m); projected DOS for a Fe_I atom (b), (f), (j), and (n); projected DOS for a Fe_{II} atom (c), (g), (k), and (o); and projected DOS for a Se atom (d), (h), (l), and (p) for the Fe(1 1 1) surface after Se adsorption.

3. Results and discussion

3.1. Surface geometry, energy and magnetic properties

Les us first compare our results with previous DFT calculations and experimental data on pure bcc iron surfaces. Table 1 presents

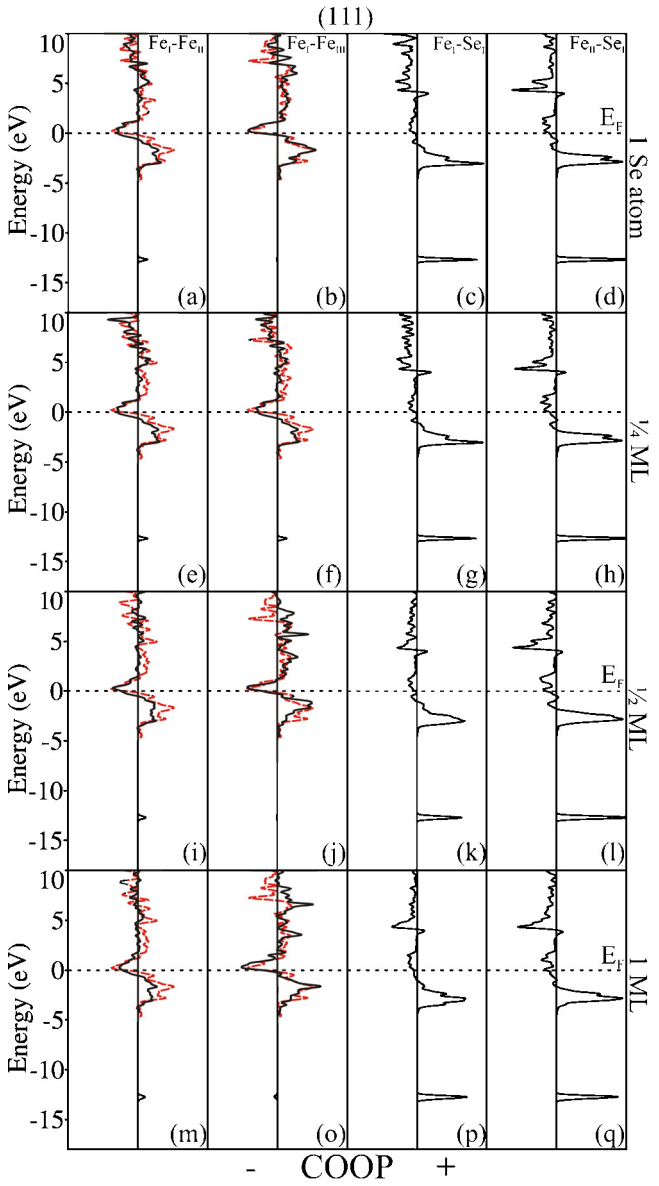

Fig. 7. COOP curves for the Fe_I–Fe_{II} bond before (black solid line) and after Se adsorption (dotted red line) (a), Fe_I–Fe_{III} bond before (black solid line) and after Se adsorption (dotted red line) (b), Fe_I–Se bond (c), and Fe_{II}–Se bond. (e)–(h), (i)–(l) and (m)–(q), the same bonds at 1/4, 1/2, and 1 ML on Fe(1 1 1) (For interpretation of the color information in this figure legend, the reader is referred to the web version of the article.).

Table 2
Adsorption energy of one Se atom on Fe(1 0 0) and Fe(1 1 1) surfaces, smallest Fe–Se distance (d_{Fe-Se}) and height of the Se atom over the top Fe surface (h) for the different adsorption sites.

Surface	(1 0 0)			(1 1 1)			
Site	Bridge	Hollow	Top	Bridge	FCC	HCP	TOP
E_{ad} (eV)	+2.09	−5.25	−3.59	−10.36	−6.16	−6.69	−8.61
d_{Fe-Se} (Å)	–	2.472	2.100	2.322	2.889	2.833	2.100
h (Å)	–	1.280	2.100	1.435	1.700	1.600	2.100

the computed relaxation, surface energy per unit area, magnetic moment per atom for the outmost Fe layer, and surface roughness. It can be seen that layer separation between the first and second Fe layer, Δ_{12}, contracts for both crystal planes considered. Relaxation on Fe(1 0 0) is much lower (−5.4%) when compared to that on Fe(1 1 1) (−26.9%) which is in full agreement with LEED measurements [39], medium-energy ion scattering (MEIS) [40] and DFT calculations [41]. The calculated surface energies are ordered as $\gamma^{111} > \gamma^{100}$, i.e., they increase with surface roughness. The abrupt termination of the metal surface and the reduced coordination of atoms in surface layers lead to the enhancement of magnetism in all surfaces considered. The values of magnetic moments on the top surface layer decrease in the following sequence (1 0 0)>(1 1 1)>(1 1 0). This behavior can be related to the correlation number of Fe atoms at the first and second layers. Thus, the number of unsaturated bonds in particular layers is crucial in the ordering of surface magnetic moment enhancement. These results are in full agreement with those reported by Błoński and Kiejna [41]. The difference between spin up and spin down contributions in the DOS for a surface Fe atom in the d band near E_F is also related to the changes in the magnetic moment (compare Fig. 3(b) and (e)).

Se adsorption energy values are all negative, except in the (1 0 0) surface bridge site, thus indicating that the adsorption is energetically favourable at low coverage (see Table 2). The most stable site is a distorted bridge on the (1 1 1) surface (−10.36 eV), its adsorption energy is almost the double when compared to Se on a long bridge site on Fe(1 1 0) (−5.25 eV) [20] and Se on the most stable site on the Fe(1 0 0) surface (−5.23 eV in a 4-fold hollow site).

The computed Fe–Se distances are between 2.100 and 2.889 Å. Se atoms are located between 1.280 and 2.100 Å above the surfaces. Similar values were determined for Se on the Fe(1 1 0) surface [20] and for sulphur belonging to the same chemical group [9–12]. Unfortunately, there are no experimental data available for a direct comparison for Se.

When considering Se coverage, adsorption energy increases at 1/4 ML compared to a single Se atom. The energy values change from −10.36 to −13.68 eV and from −5.25 to −5.36 eV on the bridge site in Fe(1 1 1), and on the hollow site in Fe(1 0 0), respectively. At a higher coverage (1 ML), the adsorption energy decreases from −10.36 to −5.56 eV and from −5.25 to −3.59 eV for the (1 1 1) and (1 0 0) surface plane, respectively.

The effect of Se on surface relaxation is different to that reported on the Fe(1 1 0) surface [20]. At 1/4 ML on the Fe(1 0 0) surface, Fe atoms contract between −1.7% and −2.0% of the interlayer distances, at 1/2 ML the contraction is −2.9%. The situation changes at 1 ML showing an outward relaxation of 4.5%. Considering the (1 1 1) surface at 1/4 ML, Se contracts the top Fe layer between −6.7% and −14.9%. At 1/2 ML some surface Fe atoms relax outwards up to 14.6% while other atoms contract −11.8%. Finally, at 1 ML all surface atoms relax outwards about 1%. In our previous calculations on the Fe(1 1 0) surface, we found that Se at 1/2 ML produces the highest displacements for Fe between +8.6% and −6.7% of the interlayer distance, followed by 1/4 ML (+2.2%, −1.61%). At 1 ML, all topmost Fe atoms relax inwards with a mean displacement of −1.69% [20].

To the best of our knowledge there is no available data for Se diffusion, from the Fe surface into the subsurface or bulk. Our preliminary calculations indicate that is not possible such diffusion unless the subsurface layers contains some Fe vacancies. Comparing Se with the isoelectronic S (which radii is smaller than Se) the results are similar. The ab initio study of S dynamics on iron surfaces of Todorova et al. conclude that S does not desorb or diffuse into the bulk at any temperature examined within simulation timeframe [42]. Barnard performed DFT calculations of S segregation on Fe and concluded that the diffusion mechanism of S is determined as the substitutional diffusion mechanism whereby a S atom diffuse from a substitutional lattice site to a nearest neighbour vacancy [43].

The magnetic moment μ in the Fe outmost layer is also modified by the presence of Se at different coverages. Table 1 shows a decrease in μ on both surfaces when the coverage goes from 1/4 to 1 ML. The most important change is detected at the (1 0 0) surface arising from 2.77 (1/4 ML) to 1.42μ_B (1 ML). Similar results were recently reported for S/Fe(1 0 0) showing that the magnetization in the top Fe layer is greatly decreased as a function of sulfur coverage, reaching as low as 1.35μ_B for 1 ML [45]. The decrease in μ at the (1 1 1) surface is small (from 2.71 to 2.56μ_B). This tendency is in agreement with those reported by Spencer et al. for S on Fe(1 1 0) [9]. The changes in the magnetic moment can be explained comparing the d band of the DOS near the Fermi level for a surface Fe atom. The DOS plot for the (1 0 0) showed an important decrease in spin up contribution for Fe_1 projected DOS when the coverage increases

Table 3
Electron orbital occupation, overlap population (OP), charge, and distances for Fe(1 0 0) before and after Se adsorption.

Structure	Electron orbital occupation			Bond type	OP	ΔOP%†	Distance (Å)
	s	p	d				
Fe(1 0 0)[a]							
Fe_1	0.74	0.30	7.40	Fe_1–Fe_2	0.314	–	2.435
Fe_2	0.69	0.32	5.99	Fe_1–Fe_3	0.180	–	2.868
Fe(1 0 0) + Se[a]							
Fe_1	0.68	0.39	7.08	Fe_1–Fe_2	0.187	−40.4	2.532
Fe_2	0.64	0.28	6.08	Fe_1–Fe_3	0.071	−60.6	3.001
Se	1.73	4.13	0.08	Fe1–Se	0.440	–	2.472
				Fe_2–Se	0.193	–	2.668
Fe(1 0 0) + Se (1/4 ML)[b]							
Fe_1	0.68	0.39	7.10	Fe_1–Fe_2	0.178	−43.3	2.556
Fe_2	0.65	0.28	6.16	Fe_1–Fe_3	0.072	−60.0	3.017
Se_1	1.73	4.12	0.08	Fe_1–Se_1	0.437	–	2.477
				Fe_2–Se_1	0.193	–	2.671
Fe(1 0 0) + Se (1/2 ML)[b]							
Fe_1	0.61	0.45	6.65	Fe_1–Fe_2	0.224	−28.7	2.458
Fe_2	0.67	0.26	6.09	Fe_1–Fe_3	0.109	−39.4	2.863
Se_1	1.71	4.05	0.10	Fe_1–Se_1	0.466	–	2.406
				Fe_2–Se_1	0.148	–	2.684
				Se_1–Se_2	0.000	–	4.044
Fe(1 0 0) + Se (1 ML)[b]							
Fe_1	0.55	0.40	6.35	Fe_1–Fe_2	0.204	−35.0	2.517
Fe_2	0.69	0.27	6.46	Fe_1–Fe_3	0.061	−66.1	2.868
Se_1	1.75	3.77	0.11	Fe_1–Se_1	0.349	–	2.424
				Fe_2–Se_1	0.092	–	2.826
				Se_1–Se_2	0.043	–	2.863

† The percentage of change is with respect to the clean surface.
[a] The geometry is shown in Fig. 1.
[b] The geometry is shown in Fig. 2.

(see Fig. 5(f), (j) and (n)). The situation is different in the case of the (1 1 1) surface where changes are very small (see Fig. 6(f), (j), and (n)).

3.2. Electronic structure and bonding for Se/Fe(1 0 0)

DOS analysis, before and after Se adsorption at a 4-fold hollow site on Fe(1 0 0) (see Fig. 1b) gives an indication of adsorbate–substrate interaction. As in the case of S [9] and in our previous study for Se/Fe(1 1 0) [20], we detected that the most affected metal orbitals are Fe 4s and 4p. The projection of Se 4p orbitals presents a contribution as a shoulder at the beginning of the Fe_1 d band (see Fig. 4(b) near −5 eV). Compared to Fe_2, second layer, the Fe–Se interaction is much lower (see Fig. 4(c)). The Se 4s orbital presents a sharp peak at −13.7 eV below E_F, this peak is 1.7 eV more stabilized than the one corresponding to Fe(1 1 0). At 1/4 ML, the DOS is similar to a single Se atom adsorption. At 1/2 ML, the Se 4s DOS peak decreases in intensity and starts broadening between −1.3 and −8.0 eV (see Fig. 4(l)). At 1 ML, the interaction with Fe_1 and Fe_2 decreases while Se based orbitals become broader and the former sharp peak at −13.7 eV becomes almost flat and spreads between −12.0 and −16.7 eV (see Fig. 4(p)). This effect is also present on the total DOS and comes from an increase in Se-Se interactions (see Fig. 4(m)). Hugosson et al. reported similar results for sulfur p and s states hybridized with the Fe (1 0 0) surface [45].

Regarding changes in the chemical bonding, COOP curves show a decrease in the area between E_F and −5 eV, which is indicative of a weakening of the Fe–Fe bond (see Fig. 5(a) and (b), compare solid black with dashed red lines) while an important Fe_1–Se bond is developed at −3.0 and −13.0 eV (see Fig. 5(c)). At 1/4 ML the behavior is similar to a single Se atom adsorption. At 1/2 and 1 ML Fe–Se bonding interaction decreases (see Fig. 5(k), (l), and (p)). The OP values for the Fe_1–Se bond change from about 0.466 to 0.349 when the coverage increases from 1/2 ML to 1 ML. We also detected a small Se–Se interaction at 2.863 Å with an OP of 0.043 (see Table 3 and Fig. 5(q)). This interaction is less developed than the one reported for the Fe(1 1 0) surface (OP 0.295 at 2.490 Å) [20] and it is not absent in the (1 1 1) plane because this is the most open surface with a mean Se-Se distance of 4.047 Å (see Table 5). The orbital by orbital contribution to the bonding between the Se atom and the surface is presented in Table 4. The Fe–Fe surface bond is made of the contributions made by s–s, s–p, p–d, and d–d. After Se adsorption, s–s and s–p interactions decrease while s–d and p–d interactions increase. For the Fe–Se bond the main contribution comes from s–p, p–p, and p–d orbitals. The Fe–Se distances lie in the range of 2.4–2.8 Å which is comparable with the (1 1 0) case (2.2–2.6 Å) [20]. The Se–Se bonding interaction distance is 2.86 Å, a little longer than that reported on Fe(1 1 0) but still close to other dimmer distances on organometallic compounds that have Se–Se bonds [20,46,47].

Table 4
Orbital by orbital percentage contributions to Fe–Fe, Fe–Se and Se–Se overlap populations (%COOP) for the Se/Fe(1 0 0) system.

	Fe_1–Fe_2		Fe_1–Fe_3		Fe_1–Se	Fe_2–Se
	Clean	Se	Clean	Se	Se	Se
Fe (1 0 0) + Se						
s–s	22.6	19.3	18.0	10.6	6.7	1.7
s–p	9.2	8.7	14.5	0.0	36.4	32.4
s–d	15.0	17.2	14.8	14.8	1.9	0.0
p–p	1.4	0.9	6.6	13.7	27.6	24.6
p–d	24.1	26.3	33.2	40.0	22.2	38.0
d–d	27.7	27.6	12.9	20.9	5.2	3.3

	Fe_1–Fe_2		Fe_1–Fe_3		Fe_1–Se_1	Fe_2–Se_1	Se_1–Se_2
	Clean	Se	Clean	Se	Se	Se	
Fe (1 0 0) + Se 1/4 ML							
s–s	22.6	19.4	18.0	9.5	6.7	1.8	–
s–p	9.2	8.4	14.5	0.0	36.3	32.9	–
s–d	15.0	17.1	14.8	14.1	1.8	0.2	–
p–p	1.4	1.2	6.6	13.9	27.7	25.6	–
p–d	24.1	27.4	33.2	39.6	22.2	36.1	–
d–d	27.7	26.5	12.9	22.9	5.3	3.4	–

	Fe_1–Fe_2		Fe_1–Fe_3		Fe_1–Se_1	Fe_2–Se_1	Se_1–Se_2
	Clean	Se	Clean	Se	Se	Se	
Fe (1 0 0) + Se 1/2 ML							
s–s	22.6	17.7	18.0	12.2	7.2	2.2	–
s–p	9.2	7.4	14.5	0.4	35.5	31.7	–
s–d	15.0	15.9	14.8	17.8	1.8	0.3	–
p–p	1.4	4.0	6.6	9.7	24.1	25.9	–
p–d	24.1	25.2	33.2	32.8	25.7	36.7	–
d–d	27.7	29.8	12.9	27.1	5.7	3.2	–

	Fe_1–Fe_2		Fe_1–Fe_3		Fe_1–Se_1	Fe_2–Se_1	Se_1–Se_2
	Clean	Se	Clean	Se	Se	Se	
Fe (1 0 0) + Se ML							
s–s	22.6	18.2	18.0	8.4	6.5	2.0	0.0
s–p	9.2	8.9	14.5	0.0	37.5	28.3	0.0
s–d	15.0	19.1	14.8	16.4	3.5	0.7	0.8
p–p	1.4	4.1	6.6	9.1	11.1	31.7	80.1
p–d	24.1	25.8	33.2	30.3	34.9	34.7	18.9
d–d	27.7	23.9	12.9	35.8	6.5	2.6	0.2

Table 5
Electron orbital occupation, overlap population (OP), charge, and distances for Fe(1 1 1) before and after Se adsorption.

Structure	Electron orbital occupation			Bond type	OP	ΔOP%[†]	Distance (Å)
	s	p	d				
Fe(1 1 1)[a]							
Fe_I	0.75	0.32	6.98	Fe_I–Fe_{II}	0.441	–	2.413
Fe_{II}	0.74	0.37	6.45	Fe_I–Fe_{III}	0.448	–	2.412
Fe(1 1 1) + Se[a]							
Fe_I	0.68	0.40	6.90	Fe_I–Fe_{II}	0.248	−43.8	2.431
Fe_{II}	0.64	0.39	5.79	Fe_I–Fe_{III}	0.425	−5.1	2.449
Se	1.76	4.45	0.04	Fe_I–Se	0.483	–	2.487
				Fe_{II}–Se	0.536	–	2.322
Fe(1 1 1) + Se (1/4 ML)[b]							
Fe_I	0.68	0.40	6.90	Fe_I–Fe_{II}	0.243	−44.9	2.440
Fe_{II}	0.64	0.39	5.80	Fe_I–Fe_{III}	0.433	−33.0	2.445
Se_I	1.76	4.45	0.04	Fe_I–Se_I	0.479	–	2.493
				Fe_{II}–Se_I	0.542	–	2.318
Fe(1 1 1) + Se (1/2 ML)[b]							
Fe_I	0.62	0.49	6.84	Fe_I–Fe_{II}	0.245	−44.4	2.491
Fe_{II}	0.64	0.39	5.65	Fe_I–Fe_{III}	0.361	−19.6	2.543
Se_I	1.75	4.36	0.05	Fe_I–Se_I	0.461	–	2.501
				Fe_{II}–Se_I	0.572	–	2.277
Fe(1 1 1) + Se (1 ML)[b]							
Fe_I	0.61	0.50	6.55	Fe_I–Fe_{II}	0.221	−49.9	2.510
Fe_{II}	0.64	0.38	5.87	Fe_I–Fe_{III}	0.382	−14.9	2.430
Se_I	1.74	4.41	0.05	Fe_I–Se_I	0.523	–	2.423
				Fe_{II}–Se_I	0.543	–	2.297
				Se_I–Se_{II}	0.000	–	4.047

[†] The percentage of change is with respect to the clean surface.
[a] The geometry is shown in Fig. 1.
[b] The geometry is shown in Fig. 2.

3.3. Electronic structure and bonding for Se/Fe(1 1 1)

The Se DOS plot also presents the 4p orbital interaction at the beginning of the Fe_I d band and sharp peak for the Se 4s orbital at −13.0 eV (see Fig. 6(a) and (d)). The stabilization of the Se states is similar to the (1 0 0) case. As the coverage increases from 1/4 to 1 ML, there is almost no broadening neither in the d band region nor in the Se 4s region (see Fig. 6(h), (l), and (p)). The DOS near the Fermi level increase due to Se contributions. The COOP curves also showed a decrease in the Fe_I–Fe_{II} OP in the d band-due to the geometry of this surface there is no Fe–Fe interaction possible in the plane, see Fig. 7(a)). Two Fe–Se bonding peaks are present at −3.0 and −13.0 eV (see Fig. 7(d)). At a higher coverage, the Fe_I–Se OP shows some decrease. Table 5 indicates a weakening in the Fe_I–Fe_{II} bond, which is near 50% in all coverages. The Fe_I–Se_I bond length goes from 2.493 Å (one Se atom) to 2.297 Å (1 ML). The orbital by orbital contribution to the Fe–Se bonding is similar to the (1 0 0) case with some increase in the d–d contribution for the Fe_I–Fe_{II} bond after Se adsorption (see Table 6).

There are some differences and some similarities between the (1 0 0) and (1 1 1) cases. The main difference in the DOS plot is the hybridization in the Se states on Fe(1 0 0) that is also present in the (1 1 0) plane and it is not detected in the (1 1 1) surface. There is also an increase in the DOS near the Fermi level coming from Se atoms in the (1 1 1) and (1 1 0) cases, this is not present in the (1 0 0) surface.

Table 6
Orbital by orbital percentage contributions to Fe–Fe and Fe–Se overlap populations (%COOP) for the Se/Fe(1 1 1) system.

	Fe_I–Fe_{II}		Fe_I–Fe_{III}		Fe_I–Se	Fe_{II}–Se
	Clean	Se	Clean	Se	Se	Se
Fe (1 1 1) + Se						
s–s	18.7	16.6	18.5	18.1	5.6	6.8
s–p	13.2	9.5	13.0	12.5	37.4	40.1
s–d	11.7	15.2	11.8	13.5	1.3	2.2
p–p	4.2	2.8	4.1	3.5	27.6	16.0
p–d	25.6	23.8	25.1	24.6	24.6	31.2
d–d	26.6	32.1	27.5	27.8	3.5	3.7
	Fe_I–Fe_{II}		Fe_I–Fe_{III}		Fe_I–Se_I	Fe_{II}–Se_I
	Clean	Se	Clean	Se	Se	Se
Fe (1 1 1) + Se 1/4 ML						
s–s	18.7	16.7	18.5	17.9	5.5	6.8
s–p	13.2	9.7	13.0	12.5	37.4	40.2
s–d	11.7	15.4	11.8	13.3	1.2	2.3
p–p	4.2	2.8	4.1	3.6	28.0	15.9
p–d	25.6	24.2	25.1	24.4	24.4	31.0
d–d	26.6	31.2	27.5	28.3	3.5	3.7
	Fe_I–Fe_{II}		Fe_I–Fe_{III}		Fe_I–Se_I	Fe_{II}–Se_I
	Clean	Se	Clean	Se	Se	Se
Fe (1 1 1) + Se 1/2 ML						
s–s	18.7	14.6	18.5	16.4	5.2	7.5
s–p	13.2	9.1	13.0	13.9	37.8	39.2
s–d	11.7	15.0	11.8	15.1	1.2	2.3
p–p	4.2	3.8	4.1	4.3	28.7	14.4
p–d	25.6	25.9	25.1	26.0	23.4	32.9
d–d	26.6	31.6	27.5	24.3	3.7	3.7
	Fe_I–Fe_{II}		Fe_I–Fe_{III}		Fe_I–Se_I	Fe_{II}–Se_I
	Clean	Se	Clean	Se	Se	Se
Fe (1 1 1) + Se ML						
s–s	18.7	14.3	18.5	15.5	6.4	7.4
s–p	13.2	8.8	13.0	9.4	37.6	38.2
s–d	11.7	15.1	11.8	15.9	1.5	2.1
p–p	4.2	4.4	4.1	2.3	26.2	16.3
p–d	25.6	26.3	25.1	20.9	24.4	31.9
d–d	26.6	31.1	27.5	36.0	3.9	4.1

Fe–Se bond lengths lie between 2.2 and 2.6 Å in all planes. A Se–Se bonding interaction is computed only in the (1 0 0) surface at 1 ML with a bond distance of about 2.863 Å which is similar that those reported for the Organoselenium compounds [46] and for the $NiS_{2-x}Se_x$ series [47]. According to the OP value, this bonding is less developed than the one previously calculated on Fe(1 1 0) at 2.49 Å [20]. In the case of the (1 1 1) surface, no Se-Se interaction is detected.

The Fe–Fe bond weakening is higher in the (1 0 0) case when compared to the (1 1 1) case, but lower than the (1 1 0) surface. The Fe–Fe bond between the first and second layer increased in (1 1 0) [20] while current calculations show a decrease in both (1 0 0) and (1 1 1) surfaces.

As mentioned before the surface reconstruction after Se adsorption is different among the surfaces studied. In the (1 0 0) case, there is some contraction (∼3% for 1/4 and ∼2% for 1/2 ML) and some outward relaxation for 1 ML (∼4%). In the (1 1 1) case at 1/4 ML the contraction is higher and approximately between −6% and −15%. At 1/2 ML some atoms go up and down irregularly while there is almost no change in the 1 ML. This behavior is different from that in the (1 1 0) case where a sort of roof-top regular movement was computed [20]. The outmost surface Fe atom magnetic moment decreases with the coverage in the following order (1 0 0) > (1 1 0) > (1 1 1).

4. Conclusions

By using periodic DFT calculations we found that the most stable Se/Fe adsorption site is a distorted bridge site on the (1 1 1) surface that almost doubles its energy when compared to the (1 0 0) and (1 1 0) surface. It also increases with coverages from −10.36 to −13.68 eV at 1/4 ML on the (1 1 1) plane. A DOS decrease at the Fermi level in the case of the (1 0 0) plane is related to the decrease in the magnetic moment on the Fe atom on the surface when coverage increases. Se–Se interaction is only detected at 1 ML coverage on the (1 0 0) surface with less OP than in the previous calculations made on the (1 1 0) surface. Our calculations predict that it is possible to achieve a decrease of about 50% in the magnetic moment on the Fe(1 0 0) surface after Se adsorption. However, the most stable Se adsorption occurs on the Fe(1 1 1) surface. If the design parameter were the magnetic moment, the samples might be mainly oriented towards the (1 0 0) direction just to avoid losing some Se on other surfaces.

Acknowledgements

Our work was supported by SGCyT-UNS and PICT 1770, PIP-CONICET No. 114-200901-00272 and No. 114-200901-00068, Grant MHES-MINCyT SLO/11/07 and CIC Buenos Aires Province A. Juan, E.A. González, P.V. Jasen and J.S. Ardenghi are members of CONICET. P. Bechthold is a CONICET fellow.

References

[1] W. Zhang, Y. Xu, L. Yuan, J. Cai, D. Zhang, Microwave absorption and shielding property of composites with FeSiAl and carbonous materials as filler, J. Mater. Sci. Technol. 28 (2012) 913–919.
[2] B.S. Batic, M. Jenko, Orientation-dependent ion beam sputtering at normal incidence conditions in FeSiAl alloy, J. Vac. Sci. Tech. A 28 (2010) 741–744.
[3] D.S. Petrovic, M. Jenko, M. Jeram, F. Marinšek, V. Prešern, Površinska segregacija elemenata onečišćivača (ugljik, bakar, fosfor, sumpor, arsen, antimon i kositar) iz slitina za neorijentirane elektrolimove (1260), Strojarstvo 48 (2006) 45–50.
[4] X.G. Ma, J.J. Jiang, S.W. Bie, L. Miao, C.K. Zhang, Z.Y. Wang, Electronic structure and magnetism of Fe_3A1_{1-x} Si_x alloys, Intermetallics 18 (2010) 2399–2403.
[5] A. Juan, R. Hoffmann, Hydrogen on the *Fe*(1 1 0) surface and near bulk bcc Fe vacancies. A comparative bonding study, Surf. Sci. 421 (1999) 1–16.
[6] M. Jenko, M. Godec, H. Viefhaus, H.J. Grabke, Antimony, tin and selenium segregation in FeSiC alloys, Mater. Sci. Forum 294–296 (1998) 747–750.

[7] M. Jenko, J. Fine, D. Mandrino, Effects of selenium surface segregation on the texture of a selenium-doped FeSi alloy, Surf. Int. Anal. 30 (2000) 350–353.
[8] H.D. Shih, F. Jona, D.W. Jepsen, P.M. Marcus, Metal-surface reconstruction induced by adsorbate: Fe(1 1 0)p(2 × 2)-S, Phys. Rev. Lett. 46 (1981) 731–734.
[9] M.J.S. Spencer, A. Huang, H.K. Snook, I. Yarovsky, Sulfur adsorption on Fe(1 1 0): a DFT study, Surf. Sci. 540 (2003) 420–430.
[10] M.J.S. Spencer, H.K. Snook, I. Yarovsky, Coverage-dependent adsorption of atomic sulfur on Fe(1 1 0): a DFT study, J. Phys. Chem. B 109 (2005) 9604–9612.
[11] M.J.S. Spencer, H.K. Snook, I. Yarovsky, Effect of S arrangement on Fe(1 1 0) properties at 1/3 monolayer coverage: a DFT study, J. Phys. Chem. B 110 (2006) 956–962.
[12] S.G. Nelson, M.J.S. Spencer, H.K. Snook, I. Yarovsky, Effect of S contamination on properties of Fe(1 0 0) surfaces, Surf. Sci. 590 (2005) 63–75.
[13] S.R. Chubb, W.E. Pickett, First-principles study of the electronic and magnetic structure of c(2 × 2) sulfur chemisorbed above Fe(0 0 1), Phys. Rev. B 38 (1988) 10227–10243.
[14] R. Wu, A.J. Freeman, G.B. Olson, Effects of P and B adsorbates on the Fe(1 1 1) surface, Phys. Rev. B 47 (1993) 6855–6858.
[15] S. Pick, P. Legare, C. Demangeat, Density-functional study of the chemisorption of N on and below Fe(1 1 0) and Fe(0 0 1) surfaces, Phys. Rev. B 75 (2007) 195446, 10.
[16] P. Błoński, A. Kiejna, J. Hafner, Theoretical study of oxygen adsorption at the Fe(1 1 0) and (1 0 0) surfaces, Surf. Sci. 590 (2005) 88–100.
[17] M. Çakmak, G.P. Srivastava, Ş. Ellialtıoğlu, K. Çolakoğlu, Ab initio study of the adsorption and desorption of Se on the Si(0 0 1) surface, Surf. Sci. 507–510 (2002) 29–33.
[18] S. Nakanishi, T. Horiguchi, Adsorption study of selenium on Fe(0 0 1) surfaces by means of LEED, AES and work-function measurements, Surf. Sci. 133 (1983) 605–617.
[19] A.B. Anderson, Atom superposition electron delocalization (ASED) theory for catalysis dissociative properties of Acetylene Fe on Ni(1 0 0) with coadsorbed O, S, Se and implications for Te, J. Catal. 67 (1981) 129–144.
[20] E.A. González, P.V. Jasen, M. Sandoval, P. Bechthold, A. Juan, B.S. Batic, M. Jenko, A theoretical study of Selenium adsorption on Fe(1 1 0), App. Surf. Sci. 257 (2011) 6878–6883.
[21] G. Kresse, J. Hafner, Ab initio molecular dynamics for liquid metals, Phys. Rev. B 47 (1993) 558–561.
[22] G. Kresse, J. Furthmüller, Efficient iterative schemes for ab initio total-energy calculations using a plane-wave basis set, Phys. Rev. B 54 (1996) 11169–11186.
[23] G. Kresse, J. Furthmüller, Efficiency of ab-initio total energy calculations for metals and semiconductors using a plane-wave basis set, Comput. Mater. Sci. 6 (1996) 15–50.
[24] J. Perdew, J.A. Chevary, S.H. Vosko, K.A. Jackson, M.R. Pederson, D.J. Singh, C. Fiolhais, Atoms, molecules, solids, and surfaces: applications of the generalized gradient approximation for exchange and correlation, Phys. Rev. B 46 (1992) 6671–6687.
[25] S.G. Louie, S. Froyen, M.L. Cohen, Nonlinear ionic pseudopotentials in spin-density-functional calculations, Phys. Rev. B 26 (1982) 1738–1742.
[26] Q. Ge, S.S. Jenkins, D.A. King, Localisation of adsorbate-induced demagnetisation: CO chemisorbed on Ni{1 1 0}, Chem. Phys. Lett. 327 (2000) 125–130.
[27] D. Vanderbilt, Soft self-consistent pseudopotentials in a generalized eigenvalue formalism, Phys. Rev. B 41 (1990) 7892–7895.
[28] H.J. Monkhorst, J.D. Pack, Special points for Brillouin-zone integrations, Phys. Rev. B 13 (1976) 5188–5192.
[29] M. Methfessel, A.T. Paxton, High-precision sampling for Brillouin-zone integration in metals, Phys. Rev. B 40 (1989) 3616–3621.
[30] WebElements™ Periodic Table: <www.webelements.com/>.
[31] A. Stibor, G. Kresse, A. Eichler, J. Hafner, Density functional study of the adsorption of CO on Fe(1 1 0), Surf. Sci. 507–510 (2002) 99–102.
[32] D.E. Jiang, E.A. Carter, Adsorption and diffusion energetics of hydrogen atoms on Fe(1 1 0) from first principles, Surf. Sci. 547 (2003) 85–98.
[33] A. Hung, I. Yarovsky, J. Muscat, S. Russo, I. Snook, R.O. Watts, First-principles study of metallic iron interfaces, Surf. Sci. 501 (2002) 261–269.
[34] R.F.W. Bader, Atoms in Molecules—A Quantum Theory, Oxford University Press, Oxford, 1990.
[35] J.C. Boettger, Nonconvergence of surface energies obtained from thin-film calculations, Phys. Rev. B 49 (1994) 16798–16800.
[36] V.C. Fiorentini, M. Methfessel, Extracting convergent surface energies from slab calculations, J. Phys.: Condens. Matter 8 (1996) 6525–6530.
[37] P. Ordejón, E. Artacho, J.M. Soler, Self-consistent order-N density-functional calculations for very large systems, Phys. Rev. B 53 (1996) R10441–R10444.
[38] J.M. Soler, E. Artacho, J.D. Gale, A. Garcia, J. Junquera, P. Ordejón, D.J. Sanchez-Portal, The SIESTA method for ab initio order-N materials simulation, J. Phys. Condens. Matter 14 (2002) 2745–2779.
[39] Z.Q. Wang, Y.S. Li, F. Jona, P.M. Marcus, Epitaxial growth of body-centered-cubic nickel on iron, Solid State Commun. 61 (1987) 623–626.
[40] C. Xu, D.J. O'Connor, Fe(1 1 1) surface relaxation analysis by in- and out-of-plane MEIS, Nucl. Instrum. Methods B 51 (1990) 278–282.
[41] P. Błoński, A. Kiejna, Structural, electronic, and magnetic properties of bcc iron surfaces, Surf. Sci. 601 (2007) 123–133.
[42] N. Todorova, M.J.S. Spencer, I. Yarovsky, The ab initio study of S dynamics on iron surfaces, Surf. Sci. 601 (2007) 665–671.
[43] Experimental and computational study of S segregation in Fe by Pieter Egbert Barnard, Magister Scientiae Thesis, Department of Physics, University of the Free State, Republic of South Africa, http://etd.uovs.ac.za/ETD-db//theses/available/etd-05272013121402/unrestricted/BarnardPE.pdf
[44] W.T. Geng, M. Kim, A.J. Freeman, Multilayer relaxation and magnetism of a high-index transition metal surface: Fe(3 1 0), Phys. Rev. B 63 (2001) 245401, 5.
[45] H.W. Hugosson, W. Cao, S. Seetharaman, A. Delin, Sulfur- and oxygen-induced alterations of the iron (0 0 1) surface magnetism and work function: a theoretical study, J. Phys. Chem. C 117 (2013) 6161–6171.
[46] J. Kuneš, L. Baldassarre, B. Schächner, K. Rabia, C.A. Kuntscher, D.M. Korotin, V.I. Anisimov, J.A. McLeod, E.Z. Kurmaev, A. Moewes, Metal–insulator transition in $NiS_{2-x}Se_x$, Phys. Rev. B 81 (2010) 035122, 6.
[47] J. Ruiz, R. Araz, M. Ceroni, M. Vivanco, J.F. Van der Maelen, S. Garcia-Granda, Synthesis and Se–Se bond breaking of polyselenides containing pendant diphosphine complexes of manganese(I), Organometallics 29 (2010) 3058–3061.